Flow Correlated Percolation during Vascular Remodeling in Growing Tumors

D.-S. Lee and H. Rieger
Theoretische Physik, Universität des Saarlandes, 66041 Saarbrücken, Germany

K. Bartha
Department of Medical Biochemistry, Semmelweis University, Budapest, Hungary
(Received 28 July 2005; published 7 February 2006)

A theoretical model based on the molecular interactions between a growing tumor and a dynamically evolving blood vessel network describes the transformation of the regular vasculature in normal tissues into a highly inhomogeneous tumor specific capillary network. The emerging morphology, characterized by the compartmentalization of the tumor into several regions differing in vessel density, diameter, and necrosis, is in accordance with experimental data for human melanoma. Vessel collapse due to a combination of severely reduced blood flow and solid stress exerted by the tumor leads to a correlated percolation process that is driven towards criticality by the mechanism of hydrodynamic vessel stabilization.

DOI: 10.1103/PhysRevLett.96.058104 PACS numbers: 87.18.−h, 61.43.Hv, 87.10.+e, 87.17.Aa

Tumor vasculature, the network of blood vessels in and around a growing tumor, is in many respects different from the regular vasculature in normal tissues. Hypoxia, the lack of oxygen that prevents a small tumor nucleus from further growth, induces the expression of various diffusible growth factors (GFs) by the tumor cells that trigger a coordinated response of angiogenesis—the formation of irregular blood vessels [1,2]. The expected increase in microvascular density (MVD) is usually observed in the periphery of the tumor, whereas the morphology of the vasculature in the tumor center is characterized by *decreased* MVD, dilated vessels, and regions of necrotic tumor tissue [3,4]. The resulting tumor specific capillary network is very heterogeneous, composed of dense and void regions, and has a fractal dimension different from normal arteriovenous or normal capillary networks [5].

Although on the molecular level the main actors in the angiogenic game are rapidly identified, the physical principles that determine the global morphology of the vascular network in tumor tissues are not known. Since, for instance, MVD is used as a diagnostic tool in cancer therapy [6], a quantitative understanding of the mechanism that leads to the compartmentalization of the tumor vasculature into various regions differing substantially in vessel density appears mandatory. Moreover, scale-invariant aspects such as fractal dimension are used as hints towards the nature of the growth process underlying the formation of the tumor vasculature [7]. In this Letter we propose a theoretical model for the evolution of tumor vasculature that illuminates the physical principles leading to its global morphology. The experimentally observed increase in MVD at the tumor perimeter and periphery and decrease in MVD and vessel dilation in the tumor center in human melanoma [4] appear also as the general scenario in the theoretical model that we discuss. Furthermore, we will argue that vessel collapses in the interior of the tumor lead to a percolation process which is driven towards criticality, the percolation threshold, via a mechanism of vessel stabilization by increased blood flow in the remaining vessels.

Guided by a $2d$ automaton model that two of us developed recently [8], we consider the tumor-vessel system as a dynamically evolving network or graph interacting with a tumor growth process. Although there is a large amount of work on the mathematical modeling of tumor-induced angiogenesis (for reviews, see, e.g., [9,10]), the integration of the two aspects, a growing tumor and a vascular structure dynamically evolving from a given one, has not been tried before: Previous attempts either assume a static tumor [11] or a static network topology [12], look at dynamic vascular remodeling in the absence of tumor growth [13], or use cell densities within continuum models [14] or in discretized versions [15], thereby disregarding all structural and hydrodynamic aspects.

In our model the interaction between tumor and vasculature takes place via two concentration fields: the oxygen (O_2) originating in the vessel network, and the growth factor originating in the tumor cells (TCs). A hydrodynamic flow is imprinted on the vessel network that emits O_2. TCs proliferate (die) when the local O_2 concentration is high (low). Vessels (edges) emerge when the local GF concentration is high enough, and they vanish (collapse) stochastically inside the tumor when the hydrodynamic shear force acting on the vessel walls is too low. The biological and pathophysiological motivation for the details of the model definition to follow is discussed in [8].

To be specific, we describe the topology of the vessel network by a graph $G = (V, E)$, each edge $e \in E$ representing a vessel and each node $v \in V$ a vessel junction. Here we restrict to capillary networks and do not discriminate between arteries and veins. The network G is embedded in the $3d$ Euclidean space R^3 and restricted to the cube Z of volume $\mathcal{L}^3$, which is discretized into $L^3 = (\mathcal{L}/a)^3$ unit cells. The microscopic length scale is chosen to be $a = 10\ \mu$m, the typical size of the endothelial cell

 © 2006 The American Physical Society

(EC) and TC. For computational convenience we restrict the edges to run only parallel to the three coordinate axes and identify an edge with the string of unit cells of Z that it covers. We assume the original tissue to be regularly vascularized with a homogeneous capillary network of given MVD that is fixed by intercapillary distance δ.

The tumor is represented by the set T of tumor cells. Initially it is a nucleus with N_{TC} tumor cells centered at $\mathbf{r}_c = (L/2, L/2, L/2)$ grown using the Eden rule [16]. The time that a TC spent under hypoxia is $t_{\mathrm{uo}}(\mathbf{r})$.

The vessel network G is the source of an O_2 concentration field $O_2(\mathbf{r})$, and the tumor T is the source of a growth factor concentration field $\mathrm{GF}(\mathbf{r})$. For computational tractability (cf. [17]) we assume a constant transmural O_2 pressure difference at all vessel walls, which implies a fixed O_2 secretion rate. This assumption overestimates the O_2 concentration in regions with high MVD, but this does not alter the model outcome significantly.

$$\mathrm{O}_2(\mathbf{r}) = \sum_{e\in E}\sum_{\mathbf{r}'\in e} h_{R_{\mathrm{oxy}}}(|\mathbf{r}-\mathbf{r}'|),$$
$$\mathrm{GF}(\mathbf{r}) = \sum_{\mathbf{r}'\in T} h_{R_{\mathrm{gf}}}(|\mathbf{r}-\mathbf{r}'|). \tag{1}$$

R_{gf} and R_{oxy} are the growth factor and O_2 diffusion radii, respectively, and for simplicity we choose a piecewise linear and normalized form for the contribution $h_R(r)$ of each tumor cell or vessel segment, $h_R(r) = (1 - r/R)/(\pi R^3/3)$ for $r < R$ and $h_R(r) = 0$ for $r \geq R$, satisfying $\int_0^\infty dr h_R(r) 4\pi R^2 = 1$.

Each edge e represents a tubular vessel of diameter $d(e)$ [initially $d(e) = 10\ \mu$m] and length $\ell(e)$, carrying a hydrodynamic blood flow $q(e)$ that exerts a shear force $f(e)$ upon the vessel walls. The flow is assumed to be incompressible, laminar, and stationary; then $q(e)$ and $f(e)$ follow Poiseuille's law: $q(e) = d^4(e)\nabla P(e)$ and $f(e) = d(e)\nabla P(e)$, where the blood pressure $P(\mathbf{r})$ in the nodes (vessel junctions) is computed using Kirchhoff's law and $\nabla P(e) = [P(\mathbf{r}_{e,i}) - P(\mathbf{r}_{e,f})]/\ell(e)$, with $\mathbf{r}_{e,i}$ and $\mathbf{r}_{e,f}$ the end points of e. The boundary condition for $P(\mathbf{r})$ on ∂Z is static and chosen such that $q(e)$, $f(e)$, and the resulting O_2 concentration are initially homogeneous (with values q_0, f_0 and $\bar{\mathrm{O}}_2$, respectively), imprinting a global net flow in the diagonal direction $\mathbf{r}_c$ (cf. [8]).

Starting with the initial configuration described above the following updates are performed sequentially in each time step of duration $\Delta t = 1$ h; cf. Fig. 1 for illustration. (a) TC proliferation: ($T \to T \cup \{\mathrm{r}\}$) at tumor surface sites $\mathbf{r}$ [16] with probability $p_{\mathrm{TC}}^{\mathrm{new}}$ if $O_2(\mathbf{r})$ is larger than a threshold c_{oxy}. (b) TC death: TCs survive a time t_{max} in an underoxygenated state, and then they die: If $t_{\mathrm{uo}}(\mathbf{r}) > t_{\mathrm{max}}$, $T \to T - \{\mathbf{r}\}$ with probability $p_{\mathrm{TC}}^{\mathrm{death}} = 1/2$. Otherwise, $t_{\mathrm{uo}}(\mathbf{r}) \to t_{\mathrm{uo}}(\mathbf{r}) + 1$ if $O_2(\mathbf{r}) \leq c_{\mathrm{oxy}}$. (c) Vessel growth: In regions of large GF concentration new vessels of maximum length ℓ_{max} form: Insert a new vessel e between two existing ones with probability $p_{\mathrm{EC}}^{\mathrm{new}}$ if $\mathrm{GF}(\mathbf{r}) > c_{\mathrm{gf}}$ at the start point $\mathbf{r}$ of the new vessel. e must not touch other vessels except at the start and the end point and $\ell(e) \leq \ell_{\mathrm{max}}$. (d) Vessel dilatation: In regions of large GF concentration vessel diameter grows (up to a maximum d_{max}): $d(e) \to d(e) + \sum_{\mathbf{r}\in e}\theta[\mathrm{GF}(\mathbf{r}) - c_{\mathrm{gf}}]/(\sum_{\mathbf{r}\in e} 2\pi)$ [where $\theta(x) = 1$ for $x \geq 0$ and zero otherwise] with probability $p_{\mathrm{EC}}^{\mathrm{dil}}$ as long as $d(e) < d_{\mathrm{max}}$. (e),(f) Vessel collapse and regression: Weakly perfused vessels can collapse due to the solid stress exerted by the tumor—after computation of $P(\mathbf{r})$, $f(e)$, and $q(e)$ vessels that are cut from the blood circulation [$q(e) = 0$] are removed. Each remaining vessel e is removed with probability $p_{\mathrm{EC}}^{\mathrm{collapse}}$ if the shear force falls below a threshold η_c: $f(e)/f_0 < \eta_c$ (cf. [13]) and more than 80% of the vessel surface sites are occupied by TCs.

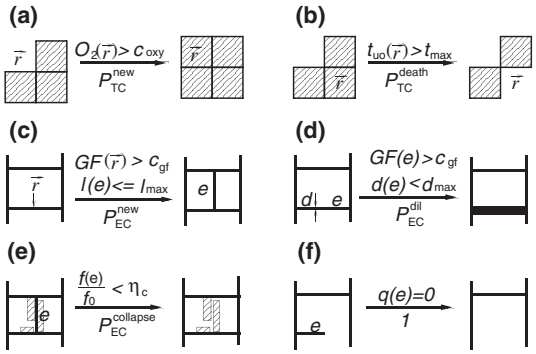

FIG. 1. Schematic illustration of the model: (a) TC proliferation, (b) TC death, (c) vessel growth, (d) vessel dilatation, (e) vessel collapse due to low shear force, and (f) collapse of uncirculated vessels.

Here we restrict ourselves to the discussion of one typical parameter set, which is partly guided by data for human melanoma [4]. The intercapillary distance is $\delta = 100\ \mu$m; i.e., MVD_0, the original MVD, is $100/\mathrm{mm}^2$. R_{oxy} is 100 μm (giving $\bar{\mathrm{O}}_2 \approx 0.03$), c_{oxy} is 0.01, and the proliferation times are for TCs $t_{\mathrm{TC}} = 10$ h (i.e., $p_{\mathrm{TC}}^{\mathrm{new}} = 0.1$) and for new vessels and vessel dilatations $t_{\mathrm{EC}} = 40$ h (i.e., $p_{\mathrm{EC}}^{\mathrm{new}} = p_{\mathrm{EC}}^{\mathrm{dil}} = 0.025$), and TC survival time $t_{\mathrm{max}} = 20$ h. We set $R_{\mathrm{gf}} = 200\ \mu$m and $c_{\mathrm{gf}} = 0.001$. d_{max} is 35 μm, $\ell_{\mathrm{max}} = 100\ \mu$m, $\eta_c = 0.5$, and the time that weakly perfused vessels can survive inside the tumor $t_{\mathrm{collapse}} = 50$ h, i.e., $p_{\mathrm{EC}}^{\mathrm{collapse}} = 0.02$. N_{TC} is 27 000.

An example for the time evolution of the tumor or vessel system in this model is shown in Fig. 2. Starting from a regular vessel network the MVD in the peritumoral region is increased due to the supply of GFs from the tumor, as can best be seen in the snapshots of an equatorial cross section through the tumor center in Figs. 2(g)–2(i). Once the tumor grows over this highly vascularized region, vessels start to collapse, by which the MVD in the interior of the tumor is continuously decreased until only a few thick vessels, surrounded by cuffs of TCs, remain. Because of the reduced MVD, the tumor center regions become hypoxic and TCs will die leaving large necrotic regions. This compartmentalization of the tumor into different shells that

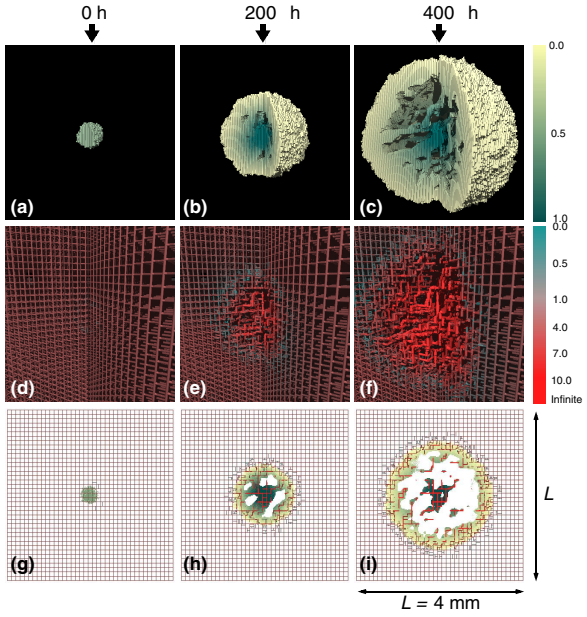

FIG. 2 (color online). The time evolution of the tumor or vessel system demonstrated by 3 snapshots at time $t = 0$, 200, and 400. (a)–(c) Only the tumor is presented (note the necrotic regions inside), (d)–(f) only the vessel network is presented (note the increased MVD at the tumor periphery, and the reduced MVD and dilated vessels in the tumor center), and (g)–(i) shows an equatorial cross section of the whole system in the xy plane at $z = L/2$. The parameter values are given in the text. The color code of the TCs represents the age scaled to $[0, 1]$ and the color code of the vessel indicates the scaled blood flow, $q(e)/q_0$.

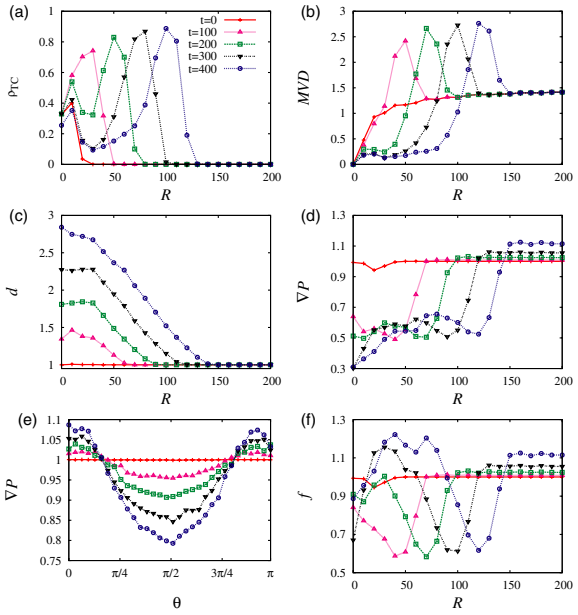

FIG. 3 (color online). (a) Tumor density ρ_{TC}, (b) MVD, (c) vessel diameter d, (d) blood pressure gradient ∇P, and (f) shear force f as a function of the distance to the center $R = |\mathbf{r} - \mathbf{r}_c|$ for different times t [see (a)]. Panel (e) shows ∇P as a function of the azimuthal angle θ. The data are averaged over all sites with the same R (or θ). Except for ρ_{TC}, all quantities are normalized to their (constant) values in the original network.

can be discriminated by MVD, vessel diameter, and necrosis is also observed in real tumors [4].

Figure 3 presents a quantitative analysis of this dynamical evolution. Shown in Fig. 3(a) is the radial tumor density $\rho_{\mathrm{TC}}(R)$. One sees that the tumor radius grows linearly with time t: $R_{\mathrm{TC}}(t) - R_{\mathrm{TC}}(0) \simeq 2t/t_{\mathrm{TC}}$, where the factor 2 is typical for the Eden growth. The radial vessel density MVD(R), shown in Fig. 3(b), has the peak in accordance with the tumor boundary at $R_{\mathrm{TC}}(t)$.

Both $\rho_{\mathrm{TC}}(R)$ and MVD(R) are substantially reduced inside the tumor due to the emergence of necrotic regions. The radial vessel diameter $d(R)$, shown in Fig. 3(c), increases linearly from 1 at $R \simeq R_{\mathrm{TC}} + R_{\mathrm{gf}}$ to $d_{\max}$ at the tumor center since vessels that have long been exposed to GFs have large diameters. Such a characteristic vessel morphology is also in a quantitative agreement with experimental data presented in [4], where the morphometry of human malignant melanoma was analyzed and the data for MVD and vessel perimeter were obtained in three different regions of the tumors: (I) the tumor center, (II) the tumor periphery, and (III) the peritumoral host tissue. It was found that for melanoma larger than 1.5 mm the MVD in (I) was less than 50% of the normal tissue MVD_0, in (II) it was around 50% more than MVD_0, and in (III) it was around 2 times MVD_0. Within the statistical error of the experimental data (up to 30%), this agrees reasonably well with our results.

Figures 3(d)–3(f) are concerned with hydrodynamic quantities: Panel (d) shows the radial blood pressure gradient $\nabla P(R)$, which is 50% lower in the tumor center than in normal vessels. This is, from hydrodynamic considerations, an immediate consequence of the increased MVD in the peritumoral region. Panel (e) shows the azimuthal dependence of the pressure gradient $\nabla P(\theta)$, where for each vessel θ is the azimuthal angle of the vessel center in a spherical coordinate system with $\mathbf{r}_c$ as center and the z axis parallel to the diagonal. $\nabla P(\theta)$ is lowest in the direction orthogonal to the global flow ($\theta = \pi/2$). Panel (f) shows the radial shear force $f(R)$, which depends on the vessel diameter and the pressure gradient. It develops a pronounced dip at the tumor boundary since the pressure gradient is reduced at the periphery but the vessel radius is increased towards the tumor center.

The qualitative behavior of our model is robust and a detailed discussion of the quantitative parameter dependencies can be found in [8] for the $2d$ case, which carries over to the present $3d$ case without substantial modifications: For example, the necrotic volume increases with the ratio $t_{\mathrm{EC}}/t_{\mathrm{collapse}}$ due to reduced O_2 supply.

The geometrical features of the emerging tumor vasculature in our model are obviously very different from the original, regular capillary network: It consists of a combination of dense and void regions that might possess fractal properties. We used the box-counting method to determine the fractal dimension D_f as $N_\varepsilon \sim \varepsilon^{-D_f}$, where N_ε is the number of boxes of volume ε^3 necessary to cover the

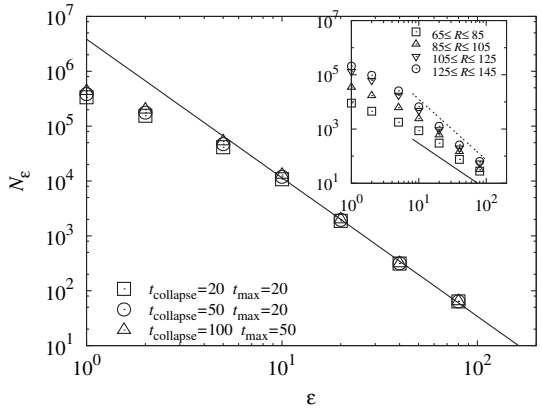

FIG. 4. Log-log plot of the box count N_ε (see text) vs ε (in units of a) for vessel networks at $t = 400$ for different values of t_{collapse} and $t_{\max}$. The straight line is the best fit $N_\varepsilon \sim \varepsilon^{-D_f}$, with $D_f = 2.52(5)$ being its slope. The local slope of the data increases monotonically from 1, the fractal dimension of an individual vessel, to its asymptotic value (cf. [19]). The inset shows N_ε of different concentric shells of thickness 20 for $t_{\text{collapse}} = 50$ and $t_{\max} = 20$. The slopes of the dashed upper line and solid lower line are -2.24 and -1.68, respectively.

tumor-vessel network lying within the outer limit of the peritumoral region $R \lesssim 145$. The plot of N_ε vs ε in Fig. 4 yields $D_f = 2.52 \pm 0.05$, which agrees with the value for the percolation cluster in conventional percolation in $3d$ [18]. We get the same value for a wide range of parameter values and at different times $t \geq 300$ and also with other methods to estimate D_f (for a discussion, including the caveats, see [19]). When we restrict the fractal analysis to concentric shells ($R_1 \leq R \leq R_2$) the estimates for D_f decrease systematically towards the tumor center (see Fig. 4, inset), reflecting the characteristic compartmentalization of the tumor vasculature also in the fractal properties.

We conclude that the basic mechanism responsible for the fractal properties of the tumor vasculature in our model is the stochastic removal of vessels via vessel collapse and regression. In conventional percolation a critical cluster emerges only for an exactly tuned bond concentration. In our model the network is dynamically driven into this critical state without such fine-tuning since the removal of vessels is correlated with the blood flow: the collapse of weakly perfused vessels stabilizes the remaining ones due to an increase in blood flow. We propose that this mechanism is also at work in real tumors. Indeed, the fractal analysis of two-dimensional photographs of vessel networks in human carcinoma yields a value of $D_f = 1.89 \pm 0.04$ [5], which agrees with D_f for the percolation cluster in $2d$ random percolation [18] and also with the value we obtain for the $2d$ version of our model [8]. It has been suggested [5] that the origin of the fractal architecture of tumor vasculature might be based on an underlying *invasion* percolation process [20] due to inhomogeneities in the growth supporting matrix. Since our theoretical model does not involve any such matrix inhomogeneities, we propose that it is rather the flow correlated percolation process that determines the fractal properties of the tumor vasculature. Neovascularization mainly occurs at the tumor perimeter, and a drastic reduction of vessel density is commonly observed in the interior of the tumor; therefore it appears unlikely that the fractal properties attained during growth in the periphery, independent of having characteristics of invasion percolation or not, survive the random dilution process in the tumor center. This suggests also for a large class of real solid tumors with decreased central MVD that the basic mechanism leading to the fractal features of the tumor vasculature is the random vessel collapse inside the tumor and not a stochastic vessel growth process.

[1] P. Carmeliet and R. K. Jain, Nature (London) **407**, 249 (2000).
[2] T. Acker and K. H. Plate, J. Mol. Med. (Berlin) **80**, 562 (2002).
[3] J. Holash *et al.*, Science **284**, 1994 (1999).
[4] B. Döme, S. Paku, B. Somlai, and J. Tímár, J. Pathol. **197**, 355 (2002).
[5] Y. Gazit *et al.*, Phys. Rev. Lett. **75**, 2428 (1995); J. W. Baish and R. K. Jain, Nature Med. **4**, 984 (1998).
[6] L. Hlatky, P. Hahnfeld, and J. Folkman, J. Natl. Cancer Inst. **94**, 883 (2002).
[7] J. W. Baish and R. K. Jain, Cancer Res. **60**, 3683 (2000).
[8] K. Bartha and H. Rieger, q-bio.TO/0506039 [J. Theor. Biol. (to be published)].
[9] N. V. Mantzaris, S. Webb, and H. G. Othmer, J. Math. Biol. **49**, 111 (2004).
[10] *Cancer Modelling and Simulation*, edited by L. Preziosi (Chapman & Hall/CRC, Boca Raton, 2003).
[11] A. R. A. Anderson and M. A. J. Chaplain, Bull. Math. Biol. **60**, 857 (1998).
[12] T. Alarcon, H. M. Byrne, and P. K. Maini, J. Theor. Biol. **225**, 257 (2003).
[13] R. Gödde and H. Kurz, Dev. Dyn. **220**, 387 (2001).
[14] H. A. Levine, B. D. Sleeman, and M. Nilsen-Hamiltion, J. Math. Biol. **42**, 195 (2001).
[15] B. Capogrosso Sansone, M. Scalerandi, and C. A. Condat, Phys. Rev. Lett. **87**, 128102 (2001).
[16] A.-L. Barabási and H. E. Stanley, *Fractal Concepts in Surface Growth* (Cambridge University Press, Cambridge, England, 1995).
[17] T. W. Secomb *et al.*, Ann. Biomed. Eng. **32**, 1519 (2004).
[18] D. Stauffer and A. Aharony, *An Introduction to Percolation Theory* (Taylor and Francis, London, 1994), revised 2nd ed.; C. D. Lorenz and R. M. Ziff, Phys. Rev. E **57**, 230 (1998).
[19] J. W. Baish and R. K. Jain, Cancer Res. **61**, 8347 (2001).
[20] L. Furuberg, J. Feder, A. Aharony, and T. Jossang, Phys. Rev. Lett. **61**, 2117 (1988); A. P. Sheppard, M. A. Knackstedt, W. V. Pinczewski, and M. Sahimi, J. Phys. A **32**, L521 (1999).